

# DualCast: Disentangling Aperiodic Events from Traffic Series with a Dual-Branch Model

Xinyu Su, Feng Liu, Yanchuan Chang, Egemen Tanin, Majid Sarvi, Jianzhong Qi  
The University of Melbourne

{suxs3@student., feng.liu1@, yanchuanc@student., etanin@, majid.sarvi@, jianzhong.qi@}unimelb.edu.au

**Abstract**—Traffic forecasting is an important problem in the operation and optimisation of transportation systems. State-of-the-art solutions train machine learning models by minimising the *mean* forecasting errors on the training data. The trained models often favour periodic events *instead of aperiodic* ones in their prediction results, as periodic events often prevail in the training data. While offering critical optimisation opportunities, aperiodic events such as traffic incidents may be missed by the existing models. To address this issue, we propose *DualCast* – a model framework to enhance the learning capability of traffic forecasting models, especially for aperiodic events. *DualCast* takes a dual-branch architecture, to disentangle traffic signals into two types, one reflecting intrinsic spatial-temporal patterns and the other reflecting external environment contexts including aperiodic events. We further propose a cross-time attention mechanism, to capture high-order spatial-temporal relationships from both periodic and aperiodic patterns. *DualCast* is versatile. We integrate it with recent traffic forecasting models, consistently reducing their forecasting errors by up to 9.6% on multiple real datasets.

**Index Terms**—Traffic series, Self-attention, Dual-branch model

## I. INTRODUCTION

Traffic series forecasting is a vital component of intelligent transportation systems (ITS) powered by the Internet of Things (IoT). It enables real-time smart urban mobility solutions [1]–[3] such as route planning as well as better transportation scheduling and mobility management strategies [4].

Deep learning-based solutions have dominated the traffic forecasting literature in recent years [5], [6]. They typically adopt graph neural networks (GNNs) for modelling spatial patterns and sequential models for modelling temporal patterns [5]–[11]. Besides, a series of recent studies adopt the attention mechanism to capture dynamic relationships in traffic patterns [6], [11]–[15].

The design of these solutions is largely driven by minimising the *mean* forecasting errors, which are an intuitive and commonly used evaluation metric [5], [11]–[13]. Implicitly, the resulting models are optimised for forecasting *periodic* traffic patterns, which are both easier to predict and prevalent in the traffic data, leading to an easier reduction in mean errors.

However, we observe substantial performance degradation from these models when facing more complex scenarios with *aperiodic* events, such as traffic incidents. Such aperiodic events are inherently challenging to predict due to their low frequency and randomness. A model capable of promptly identifying and adapting to such events will greatly enhance

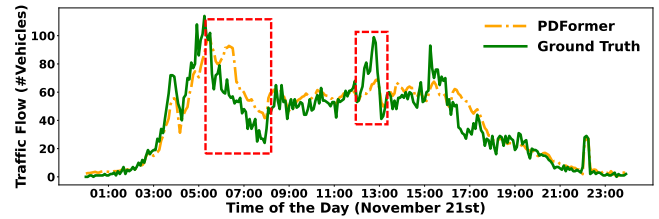


Fig. 1: An example of a recent model PDFormer [13] forecasting traffic flows for 60 minutes in advance. The model has strong overall results but fails in responding to sudden changes (highlighted by the red boxes).

the effectiveness of not only traffic forecasting but also other IoT applications in general that require real-time response to sensed signals.

Fig. 1 shows an example, where a recent model, PDFormer [13], is used to forecast the traffic flow on a freeway in California 60 minutes ahead of time for one day (detailed in Section V-B). There are two substantial gaps between the forecasts (the orange dashed line) and the ground truth (the green solid line) at around 07:00 and 13:00. These gaps would be amortised if only the mean forecasting error is examined, as the overall patterns of the two curves are quite similar.

In this paper, we propose *DualCast* – a model framework to address the issue above. *DualCast* is *not* yet another traffic forecasting model. Instead, we aim to present a **generic structure to power current traffic forecasting models with stronger learning capability to handle aperiodic patterns from traffic series**. *DualCast* has a dual-branch design to disentangle a traffic observation into two signals: (1) the *intrinsic branch* learns intrinsic (periodic) *spatial-temporal patterns*, and (2) the *environment branch* learns external environment contexts that contain aperiodic patterns. We implement *DualCast* with three representative traffic forecasting models, i.e., GMAN [12], STTN [11], and PDFormer [13], due to their reported strong learning outcomes.

The success of our dual-branch framework relies on three loss functions: *filter loss*, *environment loss*, and *DBI loss*. These functions guide *DualCast* to disentangle the two types of signals and later fuse the learning outcomes to generate the forecasting results.

(1) The **filter loss** computes the reciprocal of Kullback-Leibler (KL) divergence between the feature representations learned from two branches, ensuring that each branch captures distinct signals from the input. (2) The **environment loss** is

designed for the environment branch. It computes the reciprocal of KL divergence between a batch of training samples and a randomly permuted sequence of those samples in the same batch. This loss encourages DualCast to learn the diverse environment contexts at different times, as the samples of the training pair used in the KL divergence are drawn from different periods. (3) The **DBI loss** is designed for the intrinsic branch. It encourages DualCast to learn more separated representations for training samples with different (periodic) traffic patterns while closer representations for samples within the same traffic patterns.

As the three models [11]–[13] with which DualCast is implemented all use self-attention, we further **optimise their self-attention modules to better capture the spatial correlation across time**. We observe two issues with these existing self-attention-based models: (1) Existing self-attention-based models [11]–[13] learn spatial and temporal patterns separately. They compute attention between nodes (i.e., sensor locations with recorded traffic observations) at the same time step and between different time steps at the same node. The correlations between different nodes at different times have not been modelled explicitly, while such correlations are important for modelling the impact of aperiodic events. For example, traffic congestion caused by an incident may propagate in the road network (spatial correlations) over time (temporal correlations). (2) Existing models take either a local attention [13] or a global attention [12] setup. They compute attention only among connected nodes (based on adjacency matrix) or among all nodes. Either approach may result in limited receptive fields or loss of hierarchical relationships among the nodes (e.g., layers of traffic flow propagation).

To address these issues, we propose: (1) a *cross-time attention* module based on a (conceptual) space-time tree structure for every node starting from every time step, using hierarchical message passing. This attention mechanism computes attention between different nodes at different time steps to learn their spatial-temporal correlations, which better models traffic propagation patterns. Note that the tree structure is conceptual. It does not incur extra space costs for storage or expensive computational time costs. (2) an *attention fusion* module to fuse the local attention with the global attention, thereby enlarging the model’s receptive field and enabling the learning of the hierarchical relationships among the nodes.

Overall, this paper makes the following contributions:

(1) We propose DualCast – a model framework equipped with two branches and three loss functions to disentangle complex traffic observations into two types of signals for more accurate forecasting. DualCast is versatile in terms of the models to form its two branches – we use self-attention-based models for their reported strong learning outcomes.

(2) We propose two enhancements for self-attention-based forecasting models: (i) A cross-time attention module to capture high-order spatial-temporal correlations, and (ii) An attention fusion module to fuse global attention with local attention for enlarging DualCast’s receptive field and enabling the learning of the hierarchical relationships among the nodes.

(3) We conduct experiments on both freeway and urban traffic datasets, integrating DualCast with three self-attention-based models GMAN [12], STTN [11], and PDFormer [13]. The results show that: (i) DualCast consistently reduces the forecasting errors for these models, with stronger improvements at times with more complex environment contexts and by up to 9.6% in terms of RMSE; (ii) DualCast also outperforms the SOTA model consistently and by up to 2.6%.

## II. RELATED WORK

We briefly summarise the relevant literature on traffic forecasting models and how existing solutions (1) model correlations between different locations and times, (2) address aperiodic events, and (3) disentangle traffic series.

**Traffic forecasting models.** Traffic forecasting is a spatial-temporal forecasting problem. Initially, traffic forecasting studies focused on temporal pattern modelling [16], employing statistics time-series forecasting models such as ARIMA [17]. To better capture temporal patterns, more advanced models, such as the recurrent neural network (RNN) and its variants, are used in follow-up studies [18], [19].

Dynamic spatial correlations are considered in later studies. Since road networks can be represented as graphs, graph neural networks (GNNs)-based models [5]–[11], [20]–[23] have recently become dominant in traffic forecasting. These studies typically adopt GNNs to capture spatial features, along with RNNs [20] or 1-D temporal convolution models (TCNs) [5], [7], [9], [10] to capture temporal features. Compared with RNNs, TCNs are more efficient and can alleviate gradient explosion (or vanishing) issues in long-term forecasting.

Beyond spatial correlations, the semantic correlations between sensors also attract much attention. Different methods have been proposed to build the adjacency matrix, such as using road network distances [24], [25], node embedding similarity [9], [10], [26], time-series similarity [27], and region similarity [25], [28]. However, these adjacency matrices can only model static relationships, while real traffic patterns (e.g., traffic flows between residential and industrial areas) may vary across time. To address this gap, the attention mechanism is used in recent models to capture further dynamic (i.e., time-varying) relationships [6], [11]–[13], [15], [29] and has achieved strong outcomes. Learning different spatial correlations for different periods, such as one adjacency pattern for workday peak hours and another for weekends, is another solution [3].

**Modelling correlations between different locations at different times.** Though the models above are effective for capturing periodic patterns, they struggle with modelling aperiodic events and the ripple effect of these events, because they model the spatial and temporal correlations separately. To adapt to aperiodic events, a few GCN-based models [5], [30], [31] connect graph snapshots captured at different time steps to learn correlations between different sensor locations at different times. Such models treat impact of nodes from different hops equally, which does not reflect real-world observations where traffic propagation between nodes at different

distances takes different times. Therefore, they still struggle with capturing the propagation patterns of aperiodic events. Our proposed cross-time attention learns different weights to model such varying impacts.

**Aperiodic event-aware traffic forecasting.** Aperiodic events, such as traffic incidents and social events, are common in real-world (spatial-temporal) traffic series. Accurate forecasting with such events is important for downstream applications, e.g., transportation optimisation and route planning. However, most existing models have poor generalisation of aperiodic events. East-Net [32] and MegaCRN [26] adopt memory augment to alleviate this issue, where the memory augment (i.e., memory network) enhances model representations by learning prototype representations of spatial-temporal patterns, including aperiodic patterns. Though such memory networks can enhance model generalisation, it is difficult to predefine the number of memories to model different periodic and aperiodic patterns. Our proposed DualCast utilises environment loss to encourage the model to learn diverse aperiodic patterns without predefined numbers of aperiodic patterns, which is more flexible.

**Disentangling traffic series.** Real-world traffic series are complex and entangle multiple kinds of signals. Disentangling traffic series is an intuitive yet non-trivial task for more accurate traffic forecasting. Previous study denoises traffic data [33], while the noise could contain useful information, such as a sudden change caused by a traffic incident – ignoring such “noise” limits model generalisation. MUSE-Net [4] focuses on the disentanglement of multiple periodic signals rather than aperiodic signals. TimeDRL [34] also uses a dual-branch structure, where one learns representations at the time-stamp level (i.e., each time step in the input window has an embedding), and the other at the instance level (i.e., each input window has an embedding). A couple of other studies extract different traffic modes from traffic data using wavelet transform and decoupling [35], [36]. This approach struggles when encountering long-term aperiodic events, such as serious car accidents or major social events, which may confuse the predefined wavelets.

Disentangling and fusing high-frequency and low-frequency signals have been used to enhance model performance [37], [38]. More recent studies disentangle traffic series into invariant signals [30], [39] and environment signals, formed by a predefined set of city zones (e.g., commercial vs. residential) or environmental factors. These models are not based on self-attention, while we do. More importantly, our environment loss functions together with a dual-branch model structure enable capturing environment contexts with a higher flexibility, without the need for predefined aperiodic patterns.

### III. PRELIMINARIES

We start with the necessary background in traffic forecasting and self-attention-based traffic forecasting models.

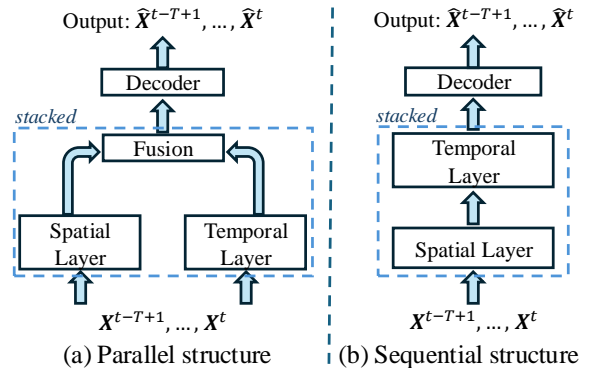


Fig. 2: Spatial-temporal forecasting model structures

#### A. Traffic Forecasting

We model a network of traffic sensors as a graph  $G = (V, E, \mathbf{A})$ , where  $V$  denotes a set of  $N$  nodes (each representing a sensor) and  $E$  denotes a set of edges representing the spatial connectivity between the sensors based on the underlying road network.  $\mathbf{A} \in \mathbb{R}^{N \times N}$  is an adjacency matrix derived from the graph. If  $v_i, v_j \in V$  and  $(v_i, v_j) \in E$ , then  $\mathbf{A}_{i,j} = 1$ ; otherwise,  $\mathbf{A}_{i,j} = 0$ .

For each sensor (i.e., a *node* hereafter, for consistency)  $v_i \in V$ , we use  $x_{i,t} \in \mathbb{R}^C$  to represent the traffic observation of  $v_i$  at time step  $t$ , where  $C$  is the number of types of observations, e.g., traffic flow and traffic speed. Further,  $\mathbf{X}_t = [x_{1,t}, x_{2,t}, \dots, x_{N,t}] \in \mathbb{R}^{N \times C}$  denotes the observations of all nodes in  $G$  at time step  $t$ , while  $\hat{\mathbf{X}}_t \in \mathbb{R}^{N \times C}$  denotes the forecasts of the nodes in  $G$  at time step  $t$ . We use  $\mathbf{X}_{t_i:t_j}$  to denote the consecutive observations from  $t_i$  to  $t_j$ , i.e.,  $[\mathbf{X}_{t_i}, \dots, \mathbf{X}_{t_j}]$ .

**Problem statement.** Given a sensor graph  $G = (V, E, \mathbf{A})$ , a traffic forecasting model generally adopts an encoder-decoder structure to learn from the traffic observations of the previous  $T$  steps and generate forecasts for the following  $T'$  steps

$$\hat{\mathbf{X}}_{t+1:t+T'} = g_\omega(f_\theta(\mathbf{X}_{t-T+1:t})), \quad (1)$$

where  $f_\theta$  and  $g_\omega$  denote the encoder and the decoder, respectively, and  $\theta \in \Theta$  and  $\omega \in \Omega$  denote the learnable parameters.

We aim to find  $f_\theta$  and  $g_\omega$  to minimise the errors between the ground-truth observations and the forecasts:

$$\operatorname{argmin}_{\theta \in \Theta, \omega \in \Omega} \mathbb{E}_{t \in \mathcal{T}} \|g_\omega(f_\theta(\mathbf{X}_{t-T+1:t})) - \mathbf{X}_{t+1:t+T'}\|_p, \quad (2)$$

where  $\mathcal{T}$  denotes the time range of traffic observations of the dataset, and  $p$  is commonly set as 1 or 2.

#### B. Self-Attention-Based Traffic Forecasting

We describe typical structures followed by self-attention-based traffic forecasting (*STF* hereafter) models [11]–[13], [23]. Our DualCast framework and attention-based optimisations are designed to be compatible with such structures. STF models typically stack *spatial-temporal layers* (STLayers) as the *encoder*  $f_\theta$  to learn spatial-temporal correlations between nodes. The hidden representations learned by  $f_\theta$  are fed into a *decoder*  $g_\omega$  to generate the forecasting results.

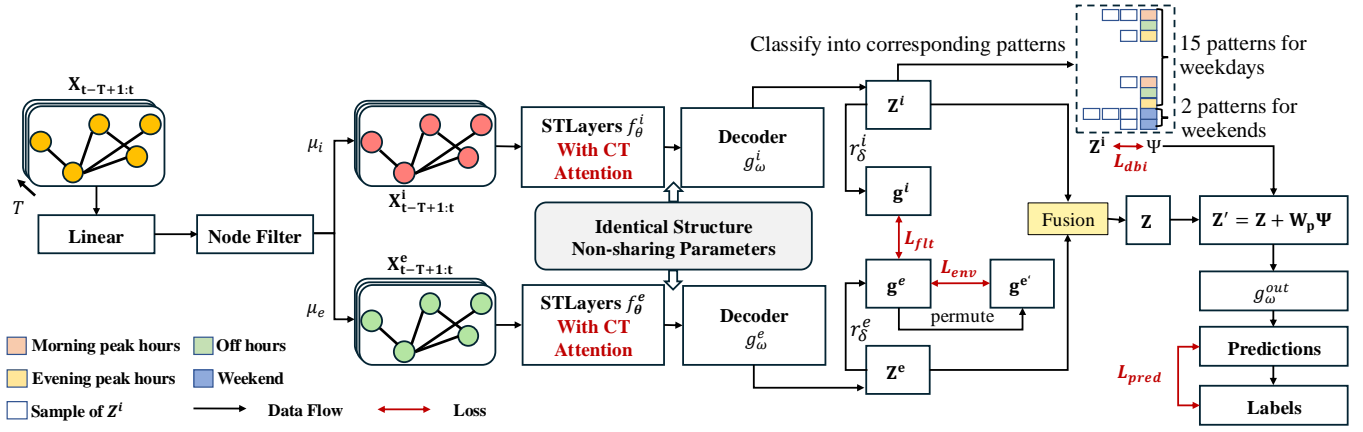


Fig. 3: The DualCast framework. DualCast maps the input traffic observations  $X_{t-T+1:t}$  ( $X$ , for simplicity) into a  $D$ -dimensional space and uses a node filter to disentangle the traffic observations into intrinsic signals ( $X^i$ ) and environment signals ( $X^e$ ). Each type of signal is fed into a separate branch (intrinsic or environment branch) formed by an encoder (STLayers with cross-time (CT) attention), a decoder, and a function to produce traffic observation representation  $Z^i$  ( $Z^e$ ) and graph representation  $g^i$  ( $g^e$ ). Three loss functions are designed to optimise DualCast: (1) The filter loss computes KL divergence between  $g^i$  and  $g^e$  to minimise their mutual information. (2) The environment loss computes KL divergence between  $g^e$  and  $permute(g^e)$  to encourage DualCast to learn different environment contexts for different times, and (3) The DBI loss promotes learning distinctive representations for different periodic traffic patterns. DualCast finally fuses  $Z^i$ ,  $Z^e$ , and  $\Psi$  to produce  $Z'$ , which is then mapped into the output space and compared with the ground truth to compute the prediction loss.

**Spatial-temporal layer.** Two structures are commonly used for the STLayers, i.e., parallel and sequential, as illustrated by Fig. 2. Parallel STLayers learn spatial and temporal features separately and then fuse the hidden representations of the two types of features to form the spatial-temporal features. In contrast, sequential STLayers process the two types of features one after another. Multiple STLayers are often stacked to learn richer spatial-temporal correlations.

**Spatial layer.** Spatial layers (SLayers) focus on the spatial correlations between sensors. The  $l$ -th SLayer projects the input (i.e., the output of the  $(l-1)$ -th STLayer) at time  $t$  into three sub-spaces:

$$\mathbf{Q}_t^{sp,l} = \mathbf{W}_q^{sp,l} \mathbf{H}_t^{l-1}, \mathbf{K}_t^{sp,l} = \mathbf{W}_k^{sp,l} \mathbf{H}_t^{l-1}, \mathbf{V}_t^{sp,l} = \mathbf{W}_v^{sp,l} \mathbf{H}_t^{l-1}. \quad (3)$$

Here,  $\mathbf{H}_t^{l-1}$  is the output of the  $(l-1)$ -th STLayer and  $\mathbf{H}_t^0 = \mathbf{X}_t$ ;  $\mathbf{W}_q^{sp,l}$ ,  $\mathbf{W}_k^{sp,l}$ , and  $\mathbf{W}_v^{sp,l}$  are learnable weights in shape  $\mathbb{R}^{D \times d}$ , where  $D$  is the dimensionality of the hidden features, and  $d$  is the dimensionality of  $\mathbf{Q}$ ,  $\mathbf{K}$ , and  $\mathbf{V}$ . Then, we compute  $\mathbf{h}_{t,n}^{sp,l} \in \mathbb{R}^d$ , i.e., the hidden representation for the  $n$ -th node (node  $n$  for brevity hereafter) at time  $t$ :

$$\mathbf{h}_{t,n}^{sp,l} = \sum_{m=1}^N \text{softmax}(\text{sim}(\mathbf{Q}_{t,n}^{sp,l}, \mathbf{K}_{t,m}^{sp,l}) \odot \mathbf{M}_{n,m}^{sp}) \mathbf{V}_{t,m}^{sp,l}. \quad (4)$$

Here,  $\text{sim}(\mathbf{X}, \mathbf{Y}) = \frac{\mathbf{X}\mathbf{Y}}{\sqrt{d}}$  is a function to compute the similarity between two matrices.  $\mathbf{M}_{n,m}^{sp}$  represents the mask between node  $n$  and node  $m$ ;  $\mathbf{M}^{sp}$  can be the matrix used by GMAN [12], the adjacent matrix based on road networks used by DCRNN [20], or the similarity matrix based on semantic representations used by PDFormer [13]. The  $l$ -th SLayer applies the self-attention across all nodes, yielding  $N$  vectors  $\mathbf{h}_{t,n}^{sp,l}$  ( $n \in [1, N]$ ), which together form matrix

$\mathbf{H}_t^{sp,l} \in \mathbb{R}^{N \times D}$ . Then, the  $l$ -th SLayer applies the self-attention at each time step and concatenates the output from each time step to produce the output of the layer  $\mathbf{H}^{sp,l} = \text{concat}(\mathbf{H}_{t-T+1}^{sp,l}, \dots, \mathbf{H}_t^{sp,l})$ .

**Temporal layer.** Temporal layers (TLayers) capture the temporal correlations of the same sensor across different time steps. For the  $l$ -th TLayer, the input is also the output the  $(l-1)$ -th STLayer, i.e.,  $\mathbf{H}_t^{l-1}$ , when STF takes the parallel structure. When STF takes the sequential structure, the input is the output of the  $l$ -th SLayer, i.e.,  $\mathbf{H}^{sp,l}$ . Similar to the SLayers, the input of node  $n$  is mapped into three sub-spaces, i.e.,  $\mathbf{Q}_n^{te,l}$ ,  $\mathbf{K}_n^{te,l}$ , and  $\mathbf{V}_n^{te,l}$ . Then, the attentions are computed as follows, where  $\mathbf{M}_{t,t'}^{te}$  is a mask to mask the messages from future time steps. The output at every time step is concatenated to form the TLayer output  $\mathbf{H}^{te,l}$ .

$$\mathbf{h}_{t,n}^{te,l} = \sum_{t'=1}^T \text{softmax}(\text{sim}(\mathbf{Q}_{t,n}^{te,l}, \mathbf{K}_{t',n}^{te,l}) \odot \mathbf{M}_{t,t'}^{te}) \mathbf{V}_{t',n}^{te,l}. \quad (5)$$

**Spatial-temporal fusion.** When STF takes the sequential structure, we do not need additional fusion, as the spatial and temporal features are naturally interacted within the TLayers. The output  $\mathbf{H}^l$  of the  $l$ -th STLayer is just  $\mathbf{H}^{te,l}$ . When STF takes the parallel structure, spatial-temporal fusion (e.g., adding, concatenating, and gating [40]) is applied to the outputs of the SLayer and the TLayer, to produce the output of an STLayer  $\mathbf{H}^l = \text{fuse}(\mathbf{H}^{sp,l}, \mathbf{H}^{te,l})$ .

**Decoder.** After the input features are processed through  $L$  (a system parameter) STLayers, the output  $\mathbf{H}^L$  of the final STLayer is fed into a decoder  $g_\omega$ , to forecast traffic conditions:

$$\hat{\mathbf{X}}_{t+1:t+T'} = g_\omega(\mathbf{H}^L). \quad (6)$$

In practice, the decoder can be made up of linear layers [13] or self-attention layers [12].

Finally, a forecasting loss, e.g., the root mean squared error (RMSE), is utilised to optimise the model with Eq. 2.

#### IV. THE DUALCAST FRAMEWORK

Next, we detail our proposed framework DualCast. As Fig. 3 shows, DualCast has a *dual branch* structure. Each branch has a *rooted sub-tree cross-time attention* (CT attention) module.

The dual-branch structure disentangles traffic observations into two types of underlying signals, namely *intrinsic (periodic) signals* and *environmental (aperiodic) signals*, which jointly contribute to accurate traffic forecasts. We introduce three loss functions: *filter loss*, *environment loss*, and *DBI loss*, to guide the model to generate distinctive representations for the two types of signals.

The rooted sub-tree cross-time attention efficiently captures dynamic and high-order spatial-temporal correlations between sensors. We explicitly learn the different correlations at different times, instead of relying on stacking STLayers as existing works do.

##### A. Dual-branches Structure and Optimisation

**Dual-branch structure.** The dual-branch structure disentangles the traffic observations into two types of underlying signals, i.e., intrinsic signals and environment signals. The two branches, i.e., the intrinsic branch (IBranch) and the environment branch (EBranch), share an identical structure but use separate parameters. The intrinsic signals reflect intrinsic (periodic) traffic patterns, while the environment signals reflect the external environment (aperiodic) contexts, such as weather, temperatures, or traffic incidents. The two signals together determine the traffic forecasts.

Given a batch of  $B$  input observations  $\mathbf{X} \in \mathbb{R}^{B \times T \times N \times C}$ , we compute *disentangling coefficients* for both types of signals:

$$\mu_i, \mu_e = \text{softmax}(\text{Linear}(\mathbf{X})), \quad (7)$$

where  $\text{Linear}$  denotes a linear layer with an output size of 2;  $\mu_i$  and  $\mu_e$  (both in shape  $\mathbb{R}^{B \times T \times N}$ ) are the disentangling coefficients for the intrinsic and the environment signals, respectively. Then, we produce the intrinsic signals  $\mathbf{X}^i = \mu_i \odot \mathbf{X}$  and the environment signals  $\mathbf{X}^e = \mu_e \odot \mathbf{X}$ , where  $\odot$  denotes element-wise product, using  $\mu_i$  and  $\mu_e$  expanded by repeating their values in the last dimension.  $\mathbf{X}^i$  and  $\mathbf{X}^e$  are then fed into IBranch and EBranch to produce the output representations  $\mathbf{Z}^i$  and  $\mathbf{Z}^e$ , respectively. We use IBranch to detail this process, while EBranch runs in the same manner.

At IBranch,  $\mathbf{X}^i$  is fed into the spatial-temporal encoder  $f_\theta^i$  to produce a hidden representation  $\mathbf{H}^i$ , which is then forwarded to the decoder  $g_\omega^i$  to produce the output representation of the branch,  $\mathbf{Z}^i \in \mathbb{R}^{B \times T \times N \times D}$ . We concatenate the outputs of both branches to obtain  $\mathbf{Z} = \text{Concat}(\mathbf{Z}^i, \mathbf{Z}^e)$  and generate the forecasts  $\hat{\mathbf{X}}$  from  $\mathbf{Z}$  through another linear layer  $g_\omega^{\text{out}}$ .

**Model training.** We use three loss functions to train DualCast: (1) a filter loss to separate the feature spaces of the two branches, (2) an environment loss to learn the impact of

environment contexts, and (3) a DBI loss to learn different periodic patterns.

**Filter loss.** The filter loss,  $L_{flt}$ , is based on KL divergence. It minimises the mutual information between the hidden spaces of the two branches to distinguish the two types of signals.

Specifically, we aggregate the output representation  $\mathbf{Z}^i$  of IBranch along the time dimension by a linear layer and the node dimension by mean pooling, to produce an overall representation  $\mathbf{g}^i \in \mathbb{R}^{B \times D}$  of each input sample. We denote this aggregation process as  $r_\delta^i$ , where  $\delta$  denotes the parameters in the linear layer. Following the same process, we can obtain  $\mathbf{g}^e$  through  $r_\delta^e$  in EBranch.

We use  $\text{softmax}(\cdot)$  to map  $\mathbf{g}^e$  and  $\mathbf{g}^i$  into distribution and compute the filter loss as follows:

$$L_{flt} = \text{KL}(\mathbf{g}^i, \mathbf{g}^e)^{-1} \quad (8)$$

**Environment loss.** The environment loss,  $L_{env}$ , guides the EBranch to learn external environment signals (aperiodic events). Our intuition is that the environment context of different samples from different time periods should be random and hence different (otherwise this becomes a periodic signal). To capture such varying environment contexts, the environment loss guides different samples to generate different environment representations. We randomly permute  $\mathbf{g}^e$  along the batch dimension to obtain  $\mathbf{g}^{e'} = \pi(\mathbf{g}^e)$ . We then obtain  $B$  sample pairs  $(\mathbf{g}_i^e, \mathbf{g}_i^{e'})$ ,  $i \in [1, B]$ . We use  $\text{softmax}(\cdot)$  to map  $\mathbf{g}^e$  and  $\mathbf{g}^{e'}$ . We aim to separate the representations of the sample pairs to guide DualCast to generate diverse environment representations for different times. Thus:

$$L_{env} = \text{KL}(\pi(\mathbf{g}^e), \mathbf{g}^e)^{-1} \quad (9)$$

**DBI loss.** The DBI loss,  $L_{dbi}$ , is inspired by the clustering metric Davies–Bouldin index (DBI) [41], to guide IBranch to learn representative intrinsic patterns.

Traffic observations have different periodic patterns at different times, e.g., workdays vs. weekends, and peak hours vs. off hours. We empirically define 17 periodic patterns based on the time, including 15 patterns for workdays (three per day: morning peak-hour, off-hour, and evening peak-hour), one for Saturdays and one for Sunday (cf. Fig. 4). Public holidays are treated as Sundays.

The output representation of IBranch,  $\mathbf{Z}^i$ , also contains  $B$  samples. We can obtain the representation for each sample by slicing  $\mathbf{Z}^i$  along the batch size dimension, i.e.,  $\mathbf{Z}^i = [\mathbf{Z}^i_1, \dots, \mathbf{Z}^i_B]$ . We classify each sample into one of the 17 patterns based on the starting time of the sample. Then, we obtain a set of sample representations for each pattern. We use  $p \in P$  to denote one such set, and  $P$  to denote the set of all 17 sets corresponding to the 17 patterns. We define a matrix  $\Psi \in \mathbb{R}^{|P| \times T \times N \times D}$  to be the prototype of the 17 patterns and optimise  $\Psi$  at model training. The intuition of  $\Psi$  is that there may be  $T$  distinct sub-patterns forming the observation of each node belonging to one of the 17 periodic patterns. Each sub-pattern is represented as a vector of size  $D$ .

The DBI loss guides DualCast to learn more separated representations for the training samples with different periodic

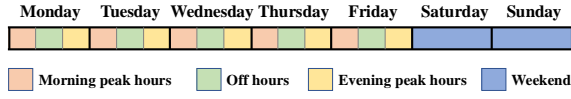


Fig. 4: Periodic patterns for the intrinsic branch.

patterns, and closer representations for those with the same periodic patterns. We first compute two metrics  $\mathcal{S}$  and  $\mathcal{P}$  that evaluate the compactness of a pattern and the separation among patterns, respectively.

$$\mathcal{S}_p(\mathbf{Z}^i, \Psi_a) = \frac{1}{|p|} \sum_{\mathbf{Z}_j^i \in p} \|\Psi_p - \mathbf{Z}_j^i\|_2. \quad (10)$$

Here,  $p$  is an element (also a set) of set  $P$ ,  $j$  is the  $j$ -th sample in  $\mathbf{Z}^i$ , and  $\Psi_p$  denotes the slicing of  $\Psi$  along the dimension of number of patterns that corresponds to  $p$ .

Next, we compute  $\mathcal{P}_{p,q}$  to evaluate the separation between sets  $p, q \in P$ ,  $\mathcal{P}_{p,q} = \|\Psi_p - \Psi_q\|_2$ .

Another metric  $\mathcal{R}_{p,q}$  balances the compactness of the two sets and the separation between them:

$$\mathcal{R}_{p,q}(\mathbf{Z}^i, \Psi) = (\mathcal{S}_p + \mathcal{S}_q) \mathcal{P}_{p,q}^{-1}. \quad (11)$$

Based on  $\mathcal{R}_{p,q}(\mathbf{Z}^i, \Psi)$ , we obtain a quality (in terms of compactness and separation) score of set  $p$ , denoted by  $\mathcal{D}_p$ :

$$\mathcal{D}_p(\mathbf{Z}^i, \Psi) = \max_{p \neq q} \mathcal{R}_{p,q}. \quad (12)$$

Finally, we can compute the DBI loss:

$$L_{dbi} = \frac{1}{|P|} \sum_{p \in P} \mathcal{D}_p(\mathbf{Z}^i, \Psi) = \frac{1}{|P|} \sum_{p \in P} \mathcal{D}_p(g_\omega^i(f_\theta^i(\mathbf{X}^1)), \Psi). \quad (13)$$

Based on the DBI loss, we can optimise prototype representations for each periodic pattern. We enhance the representation  $\mathbf{Z} = \text{Concat}(\mathbf{Z}^i, \mathbf{Z}^e)$  by aggregating  $\Psi$  as follows:

$$\mathbf{Z}' = \mathbf{Z} + \mathbf{W}\Psi. \quad (14)$$

Here,  $\mathbf{W} \in \mathbb{R}^{B \times |P|}$  is a matrix where each row contains a one-hot vector indicating the pattern set to which each sample belongs, i.e.,  $w_{j,p} = 1$  if  $\mathbf{Z}_j^i \in p$ , otherwise  $w_{j,p} = 0$ . Based on Eq. 14, we rewrite the prediction loss as follows:

$$L_{pred} = \mathbb{E}(\|g_\omega^{out}(\mathbf{Z}') - \mathbf{Y}\|_p) \quad (15)$$

**Final loss.** Our final loss combines the three loss terms above with the prediction loss (Eq. 15), using hyper-parameters  $\alpha$ ,  $\beta$ , and  $\gamma$  to control each loss term's contribution:

$$L = L_{pred} + \alpha L_{flt} + \beta L_{env} + \gamma L_{dbi}. \quad (16)$$

**Time complexity.** DualCast takes  $O(T \cdot N \cdot D^2 + \mathcal{F})$  time to map  $\mathbf{X}_{t-T+1:t}$  to  $\mathbf{X}_{t+1:t+T'}$ , where  $T$  denotes the length of the input (output) time window,  $N$  denotes the number of sensors,  $D$  is the feature dimensionality of the hidden layers, and  $\mathcal{F}$  denotes the time complexity of the spatial-temporal models (GMAN [12], STNN [11], or PDFormer [13]). Note that  $D$  is usually smaller than  $N$  in traffic forecasting tasks. Given that the time complexity of the spatial-temporal models is typically  $O(\mathcal{F}) = O(T \cdot N^2 \cdot D)$ , the time complexity of DualCast then becomes  $O(T \cdot N^2 \cdot D)$ . This time complexity

suggests that applying DualCast to power existing spatial-temporal models will not increase their time complexity, although there is a hidden constant of 2, i.e., DualCast has two branches of spatial-temporal models.

### B. Rooted Sub-tree Cross-time Attention

The rooted sub-tree cross-time attention module consists of global attention and local attention to jointly learn the high-order and dynamic spatial-temporal relationships between nodes, by learning their correlations across time. This module only applies to the spatial layers. We omit the superscript ‘ $sp$ ’ in the symbols for brevity.

Computing cross-time attention adds nodes from other time steps into the graph  $G_t$  at time  $t$ . Due to the  $O(N^2)$  time complexity for attention coefficient computation (recall that  $N$  is the number of nodes), we use a *feature mapping function* [42] that helps alleviate the high computation costs to derive the attention coefficients by the sim function (Eq. 4), i.e., Eq. 4 is replaced by:

$$\mathbf{h}_{t,n}^l = \frac{\phi(\mathbf{Q}_{t,n}^l) \sum_{m=1}^N (\mathbf{M}_{n,m} \phi(\mathbf{K}_{t,m}^l))^T \mathbf{V}_{t,m}^l}{\phi(\mathbf{Q}_{t,n}^l) \sum_{m=1}^N \mathbf{M}_{n,m} \phi(\mathbf{K}_{t,m}^l)^T}, \quad (17)$$

where  $\phi$  is a ReLU activation function;  $n$  and  $m$  denote node  $n$  and node  $m$ , respectively.

**Global attention.** We first apply Eq. 17 to compute the self-attention among all nodes at time  $t$ , obtaining  $N$  vectors  $\mathbf{h}_{t,n}^l$  ( $n \in [1, N]$ ), which form a global attention matrix  $\mathbf{H}_{t,n}^{glo}$ . As Fig. 5(c) shows, the global attention computes attention coefficients between all nodes, where  $\mathbf{M}$  in Eq. 17 is a matrix of 1’s. We then update the representations of nodes by aggregating those from all other nodes, weighted by the attention coefficients. In Eq. 17, the two summations terms  $\sum_{m=1}^N \mathbf{M}_{n,m} \phi(\mathbf{K}_{t,m}^l)^T$  and  $\sum_{m=1}^N (\mathbf{M}_{n,m} \phi(\mathbf{K}_{t,m}^l))^T \mathbf{V}_{t,m}^l$  are shared by all nodes, which are computed once. Meanwhile, we do not need to compute  $\text{sim}(\cdot, \cdot)$  in Eq. 4 any more. Thus, we reduce the time complexity from  $O(N^2)$  to  $O(N)$ .

**Local attention.** The local attention captures high-level correlations between nodes within a local area across different times. We achieve this goal by constructing an elaborate graph, where nodes from different times are connected. To learn high-level correlations, we reuse the feature mapping function-enhanced self-attention (Eq. 17), instead of the stacked spatial-temporal GNN layers, for better efficiency and effectiveness.

We use two types of edges to help learn cross-time correlations between the nodes. For a series of graph snapshots between times  $t'$  and  $t''$ , we construct (1) edges between the same node across different times (red dashed line in Fig. 5(a)), and (2) edges between a node and its one-hop neighbours from other times (green dotted line in Fig. 5(a)). This process yields a large cross-time graph with  $N|t'' - t' + 1|$  nodes and edges from the original sensor graph at every time step, and the newly created edges.

**Adjacency matrices used for local attention computation.** As Fig. 6 shows, there are two ways to build the adjacent matrices  $\mathbf{M}$  (not a matrix of 1’s any more) used in Eq. 17 for local attention computation in DualCast. In the figure,  $\mathbf{A}^1$  is

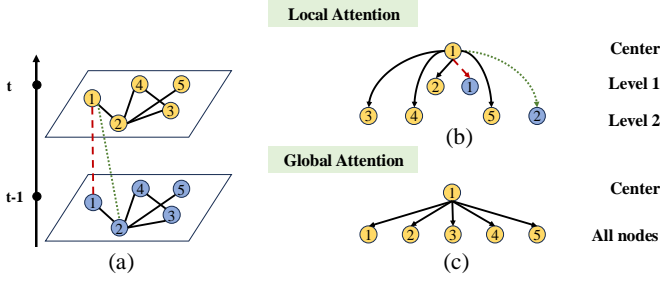


Fig. 5: Rooted sub-tree cross-time attention. For simplicity, we set  $t' - t'' = 1$ . (a) Cross-time attention. Node #1 from time step  $t$  is the root node of the subtree shown in (b). The red dashed line denotes an edge between observations of Node #1 at different times. The green dotted line denotes an edge between Node #1 and its one-hop neighbour at different times. The black lines denote edges between nodes and their one-hop neighbours observed at a time. (b) The subtree structure is used in local attention. (c) The global attention.

the original adjacency matrix that comes with the input graph  $G$  (cf. Section III-A) and  $\mathbf{A}^k$  the  $k$ -th-order matrix of  $\mathbf{A}^1$  indicating the connectivity between  $k$ -hop neighbours.

Fig 6(a) elaborates a simple way to learn high-order relationships, i.e., to pre-compute all  $k$ -hop adjacency matrices to connect all neighbours for up to  $k$  hops. However, this approach ignores the local hierarchical information. For example, the red dashed line and the green dotted line have different traffic propagation patterns and propagation time costs in Fig. 5(a), as the red dashed line only concerns the same node across different times, while the green dotted line concerns nodes at different space and times, which should not be ignored. This approach cannot such a scenario as all neighbours are considered to share the same impact, regardless of their distances (i.e., number of hops).

To fill this gap, we use a sub-tree structure. As Fig. 5(b) shows, we disentangle the attention into several levels. In the sub-tree building process, we follow the red dashed lines to form 1-hop neighbours and the green dotted lines to form 2-hop neighbours. We compute the attention weights among the neighbours of node  $n$  at level  $k$ , where  $k \in [1, \mathcal{K}]$  and  $\mathcal{K}$  denote the number of levels. Then, we aggregate representations from such neighbours to obtain  $\mathbf{h}_{t,n}^{k,loc}$  as shown in Eq. 18. After computing these representations for all nodes, we form matrix  $\mathbf{H}_t^{k,loc}$  by assembling the vectors  $\mathbf{h}_{t,n}^{k,loc}$  for  $n \in [1, N]$ . Then, we aggregate representations from all levels to obtain  $\mathbf{H}_t^{loc} = \sum_{k=0}^{\mathcal{K}} w_k \mathbf{H}_t^{k,loc}$ . Here,  $w_k$  is a learnable parameter to control the contribution of each hop.

$$\mathbf{h}_{t,n}^{0,loc} = \mathbf{V}_{t,n},$$

$$\mathbf{h}_{t,n}^{k,loc} = \frac{\phi(\mathbf{Q}_{t,n}^{sp}) \sum_{m=1}^N (\mathbf{M}_{n,m}^k \phi(\mathbf{K}_{t,m}))^T \mathbf{V}_{t,m}}{\phi(\mathbf{Q}_{t,n}) \sum_{m=1}^N \mathbf{M}_{n,m}^k \phi(\mathbf{K}_{t,m})^T}. \quad (18)$$

The above computation process can be seen as a  $k$ -hop message-passing process. Based on the  $k$ -hop message-passing

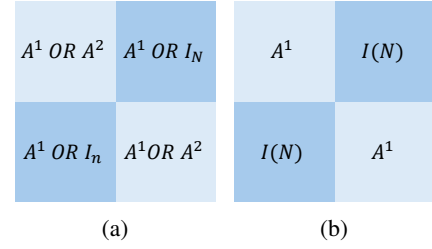


Fig. 6: Adjacency matrices for different model structures

process, the mask  $\mathbf{M}^k$  in each step equals to  $\mathbf{A}^1$ , denoted as  $\mathbf{A}$ . Fig. 6(b) shows this matrix, where  $I_N$  denotes an identity matrix of size  $N$ . During this process, we first compute  $\phi(\mathbf{K}_{t,n})$  and a message, denoted as  $\mathbf{Mess}_n = \phi(\mathbf{K}_{t,n})^T \mathbf{V}_{t,n}$ , for each node  $n$ . Then, we let  $\phi(\mathbf{K}_{t,n})$  and  $\mathbf{Mess}_n$  undergo  $k$  steps of message passing. Finally, we update the node representations by aggregating keys and values  $\sum_{m=1}^N \mathbf{A} \mathbf{Mess}_m$  and  $\sum_{m=1}^N \mathbf{A} \phi(\mathbf{K}_{t,m})$  with a node's own query  $\phi(\mathbf{Q}_{t,n})$ . Since the message-passing process runs for each edge and among all nodes, we obtain  $\mathbf{H}_t^{loc}$  with time complexity  $O(|E'|)$ . Here,  $E'$  represents the number of edges after we build the edges across graphs from different time steps (i.e., number of 1's in  $\mathbf{A}$ ). Our proposed full DualCast model uses this strategy to effectively and efficiently capture the relationships between multi-hops neighbours.

After obtaining  $\mathbf{H}_t^{loc}$  and  $\mathbf{H}_t^{glo}$ , we fuse them as follows:

$$\mathbf{H}_t = \mathbf{H}_t^{loc} + w_{glo} \mathbf{H}_t^{glo}, \quad (19)$$

where  $w_{glo}$  is a learnable parameter. Then, we concatenate  $\mathbf{H}_t$  from each time step  $t$  to obtain the output of the spatial self-attention layer  $\mathbf{H} = \parallel_{t=0}^T \mathbf{H}_t$ .

We also use a temporal self-attention module to capture the temporal features from the full input time window. As detailed in Section III-B, we merge  $\mathbf{H}^{sp}$  with  $\mathbf{H}^{te}$  to obtain the final output of the spatial-temporal layer.

**Discussion:** The high-order and dynamic spatial-temporal relationships play an important role in traffic forecasting. Previous graph-based methods [5], [8] stack GNNs to capture such correlations, with sub-optimal effectiveness, while the vanilla self-attention models suffer in their quadratic time complexity. Our work addresses these issues and presents a versatile self-attention-based method to exploit the high-order and dynamic spatial-temporal relationships effectively and efficiently.

## V. EXPERIMENTS

### A. Experimental Setup

**Datasets.** We use two freeway traffic datasets and an urban traffic dataset: **PEMS03** and **PEMS08** [43] contain traffic flow data collected by 358 and 170 sensors on freeways in North Central and San Bernardino (California), respectively, from July to August 2017; **Melbourne** [27] contains traffic flow data collected by 182 sensors in the City of Melbourne, Australia, from July to September 2022.

TABLE I: Dataset Statistics

Dataset	PEMS03	PEMS08	Melbourne
#sensors	358	170	182
#edges	547	277	398
Mean of readings	179.26	230.68	115.74
Std Dev. of readings	143.71	146.2	155.86
Median of readings	136	215	56
Starting time	09/2018	07/2016	07/2022
End time	11/2018	08/2016	09/2022
Time interval	5 min	5 min	15 min

TABLE II: Parameter Settings

Model	Parameter	PEMS03	PEMS08	Melbourne
STTN	$\alpha$	0.01	1	0.01
	$\beta$	0.01	0.01	0.01
	$\gamma$	0.5	0.05	0.1
GMAN	$\alpha$	1	5	0.05
	$\beta$	0.1	0.1	0.1
	$\gamma$	0.5	0.1	5
PDFormer	$\alpha$	0.05	0.1	0.05
	$\beta$	0.01	0.1	0.01
	$\gamma$	0.1	1	0.1

The traffic records in PEMS03 and PEMS08 are given at 5-minute intervals (288 intervals per day), while those in Melbourne are given at 15-minute intervals (96 records per day). Table I summarises the dataset statistics. As shown, Melbourne has a higher standard deviation and is more challenging.

Following previous works [9], [20], we use records from the past hour to forecast for the next hour, i.e.,  $T = T' = 1 \text{ hour}$  in Eq. 2 over all datasets. We split each dataset into training, validation, and testing sets by 7:1:2 along the time axis.

**Competitors.** DualCast works with spatial-temporal models that follow the described self-attention-based structure. We implement DualCast with three such models: **GMAN** [12], **STTN** [11], and **PDFormer** [13], denoted as **DualCast-G**, **DualCast-S**, and **DualCast-P**, respectively.

We compare with the vanilla GMAN, STTN, and PDFormer models, plus GNN-based models **GWNet** [9], **MTGNN** [22], and **STPGNN** [23]. We further compare DualCast with **MegaCRN** [26] and **EAST-Net** [32], which focus on modelling non-stationarity in spatial-temporal series. We also compare with **STWave** [36] and **STNorm** [37], which consider disentanglement in spatial-temporal forecasting.

**Implementation details.** We use the public released code of the competitors, except for STTN which is implemented from Libcity [44]. We implement DualCast with the self-attention-based models following their source code, using PyTorch.

We use the default settings from the source code for both the baseline models and their variants powered by DualCast. We train the models using Adam with a learning rate starting at 0.001, each in 100 epochs. For the models using DualCast, we use grid search on the validation sets to tune the hyper-parameters  $\alpha$ ,  $\beta$ , and  $\gamma$ . The search range  $\{0.01, 0.05, 0.1, 0.5, 1, 5\}$  follows previous works [45], [46]. Table II lists these hyper-parameter values.

All experiments are run on an NVIDIA Tesla A100 GPU with 80 GB RAM. Following [25], [30], we adopt two

common metrics – the average of root mean squared errors (**RMSE**) and mean absolute errors (**MAE**) for evaluation, which are better in complex environments with higher values. The reported results are averaged over five runs.

## B. Overall Results

**Model performance across all times.** Table III reports the forecasting errors averaged over a one-hour time span. Powered by our DualCast, DualCast-G, DualCast-P, and DualCast-S all outperform their respective vanilla counterparts consistently. DualCast-P has the best performance on freeway traffic datasets PEMS03 and PEMS08, while DualCast-G performs the best on the urban traffic dataset Melbourne. Compared to PEMS03 and PEMS08, Melbourne represents an urban environment with greater variability in the traffic flow series (cf. Table I). GMAN with a simple yet effective structure is more robust across both types of datasets, explaining for its (and DualCast-G’s) strong performance on Melbourne. PDFormer features a complex model structure that utilises time series clustering to learn typical patterns and enhance performance. While it excels over PEMS03 and PEMS08, its performance on Melbourne is suboptimal. The high variability of Melbourne makes learning effective time series clusters challenging, hindering PDFormer’s forecasting accuracy.

Among the baseline models, STWave leverages wavelet transforms to disentangle complex signals; however, its predefined wavelets can confuse long-duration events (e.g., traffic congestion caused by incidents lasting over 30 minutes) with periodic trends, leading to degraded long-term forecasting performance. MTGNN and MegaCRN are the best-performing baseline models on PEMS03 and Melbourne, respectively. MTGNN uses a graph structure learning component and adopts a mix-hop learning strategy to capture dynamic spatial relationships and learn useful neighbourhood information. MegaCRN leverages its memory bank for node embeddings, allowing it to better distinguish and capture the diverse traffic patterns entailed in Melbourne data.

We further report the RMSE for forecasting 15, 30, and 60 minutes ahead in Fig. 7. For clearer visualisation, we plot DualCast-G, DualCast-P, and DualCast-S and their vanilla counterparts, plus two other overall best-performing baselines MegaCRN and STPGNN. We see that the DualCast models outperform the baseline models consistently at different forecasting horizons, confirming their robustness.

**Model performance during hours prone to traffic accidents.** To verify that DualCast helps better learn the impact of complex environment context, we next zoom in on the forecasting results at the times with such contexts (*complex times* hereafter). Since there is no ground truth of complex times, based on studies that analyse traffic accident patterns [47], [48], we focus on 4:00 pm to 8:00 pm on workdays, which has reported a higher chance of traffic accidents. Table IV shows the results, where “all” means the RMSE at the 1-hour horizon for all days and “cpx” means that at complex times.

All models, including ours, have larger errors at complex times in most cases (except for STWave, GMAN, DualCast-

TABLE III: Overall model performance. “↓” indicates lower values are better. The best baseline results are underlined, and the best results of DualCast are in boldface. “Error reduction” denotes the percentage decrease in errors by the best DualCast-based model compared to the best baseline. The numbers in blue denote error reduction achieved by a DualCast-based model compared with the corresponding vanilla model, e.g., DualCast-P vs. PDFormer.

Model	PEMS03		PEMS08		Melbourne	
	RMSE↓	MAE↓	RMSE↓	MAE↓	RMSE↓	MAE↓
GWNet	26.420±0.839	15.404±0.052	25.796±0.318	16.314±0.230	25.778±0.136	13.410±0.065
MTGNN	<u>25.413±0.201</u>	14.707±0.070	23.794±0.073	14.898±0.066	25.364±0.291	13.310±0.137
STPGNN	25.889±0.718	14.868±0.141	23.374±0.088	14.202±0.085	25.170±0.083	13.075±0.071
MegaCRN	25.645±0.119	14.733±0.031	24.052±0.333	15.118±0.034	<u>24.482±0.143</u>	<u>12.647±0.033</u>
EASTNet	26.920±1.732	16.356±1.511	27.166±2.088	17.574±1.910	28.494±1.143	15.310±0.746
STNorm	27.328±0.437	16.382±0.191	26.026±0.119	17.090±0.113	25.744±0.277	13.724±0.134
STWave	26.346±0.174	14.975±0.086	23.270±0.108	<u>13.480±0.089</u>	26.918±0.455	14.060±0.341
STTN	27.166±0.408	15.490±0.115	24.984±0.248	15.924±0.200	26.402±0.247	13.790±0.117
GMAN	26.624±0.503	15.520±0.111	23.750±0.194	14.080±0.036	24.496±0.351	12.652±0.136
PDFormer	25.950±0.421	<u>14.690±0.080</u>	23.250±0.099	13.654±0.337	27.072±0.301	14.230±0.069
DualCast-S (ours)	26.282±0.128 (+3.3%)	15.370 ±0.086 (+0.8%)	24.526±0.116 (+1.8%)	15.550±0.119 (+2.3%)	25.474 ±0.184 (+3.5%)	13.316±0.061 (+3.4%)
DualCast-G (ours)	25.582±0.414(+3.9%)	15.094±0.099 (+2.7%)	23.564±0.133 (+0.8%)	13.938±0.114 (+1.0%)	<b>23.978±0.105 (+2.1%)</b>	<b>12.420±0.057 (+1.8%)</b>
DualCast-P (ours)	<b>24.898±0.663 (+4.1%)</b>	<b>14.666±0.087 (+0.2%)</b>	<b>22.998±0.161 (+1.1%)</b>	<b>13.332±0.059 (+2.4%)</b>	26.040±0.150 (+3.8%)	13.542±0.003 (+4.8%)
Error reduction	2.0%	0.2%	1.1%	1.1%	2.1%	1.8%

G, and DualCast-P on Melbourne). This shows that 4:00 pm to 8:00 pm is indeed a more challenging time. Importantly, the errors of the DualCast-based models increase less at complex times. The performance gap between the DualCast-based models and their respective vanilla models becomes even larger, e.g., that between DualCast-G and GMAN, and DualCast-P and PDFormer on PEMS08 double from 1.6% to 3.0% and 0.7% to 1.4%, respectively. Meanwhile, DualCast-P reduces the errors by up to 9.6% on Melbourne. These results confirm that, by disentangling the impact of intrinsic contexts and environment contexts, we can obtain more accurate traffic forecasts. We observe a few exceptions on Melbourne, because the dataset is already rather complex overall and has a large variance and skewness, such that even the supposedly not-so-complex times could be difficult to handle.

**Model scalability.** We vary the number of sensors from 200 to 1,000 in Melbourne, which expands the sensor locations from downtown to suburbs. We use Melbourne as PEMS03 and PEMS08 have bounded areas with limited sensors.

Fig. 8(a) shows the forecasting errors. Like before, the model variants powered by DualCast outperform the vanilla counterparts consistently, while the best DualCast-based model, DualCast-G, also outperforms the best baseline models. When the number of sensors grows, the errors first drop and then increase. The initial drop is because we start with sensors in the City of Melbourne, where there is a high level of variation in the traffic data leading to high forecasting errors. These high errors get amortised as more sensors from outer suburbs are added. As more and more sensors are added (e.g., over 600), the learning capabilities of the models get challenged, which causes the errors to rise again.

**Effectiveness vs. model scale.** DualCast has a dual-branch structure that increases the number of model parameters. We conduct further experiments to compare the model effectiveness between the DualCast-based models and the original models without using DualCast but with twice or triple the number of layers (such that the numbers of parameters of each pair of models differ by less than 6%), to show that DualCast is more effective than simply doubling the size of the models.

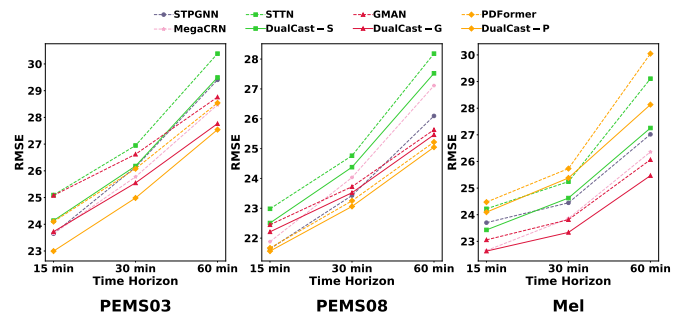


Fig. 7: Forecasting errors vs. time horizon. The dashed lines represent baseline models while the solid lines represent DualCast-based models. The green, red, and orange represents DualCast-S, DualCast-G and DualCast-P and their counterparts respectively.

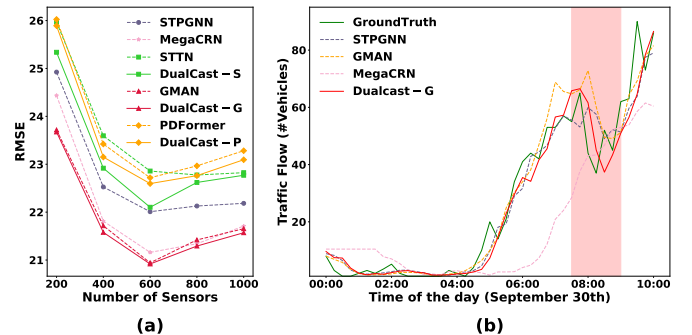


Fig. 8: (a) Forecasting errors vs. number of sensors and (b) A case study of responding to a car crash at sensor #138 on Melbourne. The occurrence time is highlighted in red.

Table V shows the results on PEMS03, where **STTN-D**, **GMAN-D**, and **PDFormer-D** denotes the model variants with twice the number of parameters of STTN, GMAN, and PDFormer, respectively. We see that these model variants are outperformed by our DualCast-based variants in RMSE, even though both types of variants share similar numbers of parameters. These results show that simply doubling the size of the models is not as effective as our dual-branch model

TABLE IV: Model performance (RMSE at the 1-hour horizon) at times with more complex environment context. “all” means model performance at any time in the day. “cpx” means model performance at times with complex environment context (4:00 pm to 8:00 pm). The best baseline results are underlined, and the best results of DualCast are in boldface. The numbers in blue denote error reduction achieved by a DualCast-based model compared with the corresponding vanilla model.

Model	PEMS03		PEMS08		Melbourne	
	all	cpx	all	cpx	all	cpx
GWNet	30.152	37.276	29.162	31.986	27.766	29.186
MTGNN	<u>27.984</u>	<u>34.842</u>	26.253	28.616	27.264	27.994
STPGNN	29.405	35.346	26.095	27.320	27.018	27.510
MegaCRN	28.472	35.692	27.110	27.442	26.360	26.654
EASTNet	30.434	37.786	31.066	32.674	31.240	33.220
ST-Norm	30.895	38.956	29.366	31.948	27.752	29.304
STWave	29.210	37.312	25.600	27.130	29.562	29.324
STTN	30.386	40.990	28.182	31.400	29.108	30.554
GMAN	28.760	36.078	25.632	26.886	26.066	25.045
PDFormer	28.542	35.416	<u>25.468</u>	27.022	30.048	30.060
DualCast-S (ours)	29.494 (+2.9%)	39.138 (+4.5%)	27.522 (+2.3%)	30.454 (+3.0%)	27.256 (+6.4%)	28.946 (+5.3%)
DualCast-G (ours)	27.766 (+3.5%)	34.450 (+4.5%)	25.464 (+0.7%)	26.506 (+1.4%)	<b>25.468 (+2.3%)</b>	<b>24.398 (+2.6%)</b>
DualCast-P (ours)	<b>27.542 (+3.5%)</b>	<b>33.950 (+4.7%)</b>	<b>25.048 (+1.6%)</b>	<b>26.224 (+3.0%)</b>	28.134 (+6.4%)	27.168 (+9.6%)
Error reduction	1.6%	2.6%	1.7%	2.5%	2.3%	2.6%

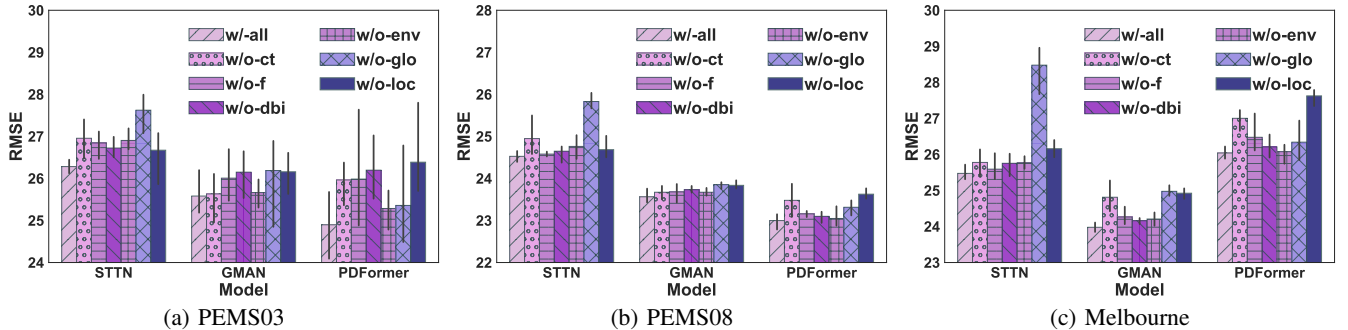


Fig. 9: Ablation study results.

TABLE V: Model Effectiveness vs. Scale (PEMS03)

Model	#Parameter	RMSE	Error reduction
STTN-D	540,581	29.960	12.3%
DualCast-S	558,252	26.282	
GMAN-D	569,667	26.590	3.8%
DualCast-G	535,804	25.582	
PDFormer-D	1,114,077	26.180	4.9%
DualCast-P	1,174,918	24.898	

design, thus emphasising the advantage of our model structure. We omit the performance results on the other two datasets as the comparative model performance patterns are similar.

### C. Ablation Study

Next, we report results to show the effectiveness of the different components of DualCast.

**Effectiveness of all DualCast components.** We implement six model variants: **w/o-ct** disables the cross-time attention from DualCast; **w/o-f**, **w/o-dbi**, and **w/o-env** remove the filter loss, the DBI loss, and the environment loss, respectively; **w/o-glo** and **w/o-loc** remove the global attention and local attention (including the cross-time attention), respectively.

As Fig. 9 shows, all modules in DualCast contribute to the overall model performance. Cross-time attention is more important for GMAN and PDFormer on Melbourne because

Melbourne data has more fluctuations (cf. Table I). Capturing high-order spatial-temporal relationships facilitates faster response to those sudden changes. On the other hand, STTN already employs GCN and self-attention to capture spatial correlations, reducing the importance of cross-time attention. Furthermore, the GCN-based spatial feature extraction effectively models local spatial features, making local attention less critical for DualCast-S compared to global attention. However, local attention is crucial for DualCast-P because PDFormer employs heterogeneous masking-based attention, which effectively captures diverse local spatial information. Ignoring local attention based on the road network structure leads to a loss of hierarchical road network information, resulting in significant performance degradation.

The DBI loss is more important on PEMS03 compared with Melbourne, because PEMS03 is a freeway dataset with more distinctive patterns across different times and days. Such patterns are to be learned by DualCast as guided by the DBI loss. Melbourne is an urban dataset with more aperiodic events, making it difficult for DualCast to learn any periodic patterns even with the DBI loss.

**Efficiency of cross-time attention.** Next, we test the attention computation efficiency. We use DualCast-G as GMAN’s own attention module is the simplest compared with PDFormer

TABLE VI: Spatial Attention Efficiency (DualCast-G)

Dataset	Model	RMSE	Time Cost (s)		
			Training	Inference	Spatial Att.
PEMS03	DualCast-G-sim	26.510	1467.9	28.0	1093.8
	DualCast-G-rct	25.900	412.8	21.5	76.6
PEMS08	DualCast-G-sim	23.727	194.3	5.9	86.1
	DualCast-G-rct	23.683	125.8	5.4	22.3
Melbourne	DualCast-G-sim	24.320	35.8	1.3	16.9
	DualCast-G-rct	24.183	23.3	0.9	6.3

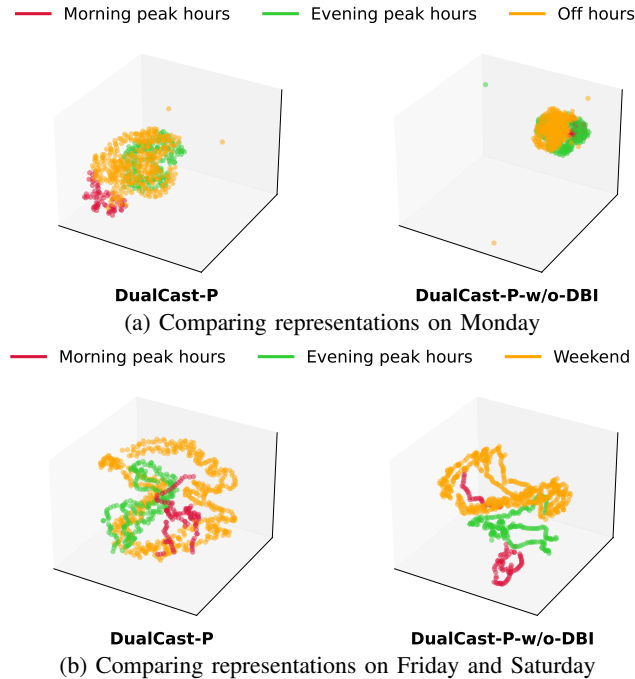


Fig. 10: t-SNE visualisation on the feature space for DualCast-P and DualCast-P-w/o-DBI on PEMS03.

and STTN, making it more suitable to observe the impact of the cross-time attention added by DualCast. We implement two variants as described in Section IV-B: (i) **DualCast-G-sim** computes the spatial self-attention based on Eq. 4 with the adjacency matrix shown in Fig. 6(a). This adjacency matrix models the relationships between neighbours within two hops at the same time step, as well as relationships between neighbours within one hop at different time steps. (ii) **DualCast-G-rct** (this is the one using our proposed rooted sub-tree attention) computes the attention and updates the representation with message-passing. This model uses the adjacency matrix shown in Fig. 6(b), which models the relationships between neighbours within one hop at the same time step and the relationships between a node and itself at different time steps.

Table VI reports the results. DualCast-G-sim takes more time for model training, inference, and attention computation, yet it has higher errors compared with DualCast-G-rct. These results confirm that our proposed rooted sub-tree attention is more efficient and effective for computing the high-order spatial-temporal correlations and the cross-time attention.

#### Effectiveness of representation learning for different

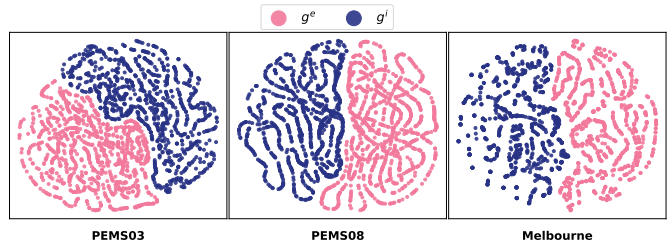


Fig. 11: t-SNE visualisation for  $g^i$  and  $g^e$  of DualCast-P.

TABLE VII: Effectiveness (RMSE) of the dual-branch structure on STTN. “Overall” means the errors averaged over 1-hour time-span. “60 min” means the errors at the 1-hour horizon for all-day time windows. “cpx” means the errors during complex times (4:00 pm to 8:00 pm).

Dataset	Method	Overall	60 min	cpx
PEMS03	STTN	27.170	30.386	40.990
	STTN-dual	26.950	29.872	39.350
Error reduction		0.8%	1.7%	4.0%
PEMS08	STTN	24.980	28.182	31.400
	STTN-dual	24.900	28.090	30.820
Error reduction		0.3%	0.3%	1.8%
Melbourne	STTN	26.400	29.108	30.550
	STTN-dual	25.770	28.360	29.000
Error reduction		2.4%	2.6%	5.1%

**patterns.** Fig. 10(a) visualises the representations learned by DualCast-P with and without the DBI loss on PEMS03 during the morning peak hour (06:00 to 09:00, in red), evening peak hour (16:00 to 22:00, in green) and off-hour (in orange) on all Mondays in the test set (same as below), to verify if the DBI loss can guide the model to distinguish traffic patterns within the same day. Fig. 10(b) further visualises representations during the morning peak hour (in red), evening peak hour (in green) on all Fridays and representations during Saturdays (in orange), to verify if the DBI loss can guide the model to distinguish traffic patterns between workdays and weekends. As the figures show, DualCast-P with the DBI loss generates representations for different times and days that are well separated, while DualCast-P-w/o-DBI mixes these representations. This result confirms the effectiveness of the DBI loss. We omit results on the other two datasets as their performance patterns are similar.

**Effectiveness of disentanglement.** To verify the effectiveness of disentanglement with our dual-branch structure, we adopt t-SNE to reduce the dimension of  $g^i$  and  $g^e$  produced by DualCast-P (recall that these are the outputs of the two branches) to 2 and visualise them in Fig. 11. The blue dots in the figure represent  $g^i$ , and the pink dots represent  $g^e$ . As the figure shows, our proposed disentanglement can separate the intrinsic signals from the environment context, further confirming the model’s effectiveness.

**Effectiveness of our dual-branch structure when applying to GCN-based models.** We further explore the application of DualCast to GCN-based models. We use STTN for this set of experiments since it utilises GCN for spatial feature

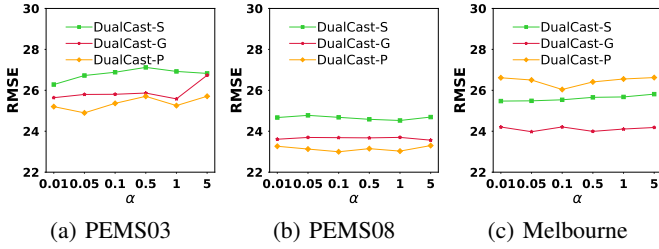


Fig. 12: Forecasting errors vs. hyper-parameter  $\alpha$  in the loss

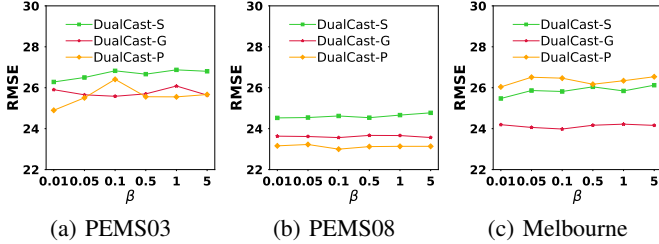


Fig. 13: Forecasting errors vs. hyper-parameter  $\beta$  in the loss

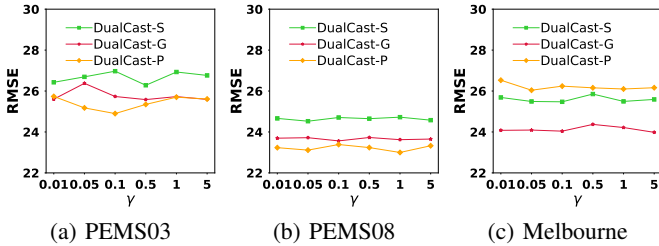


Fig. 14: Forecasting errors vs. hyper-parameter  $\gamma$  in the loss

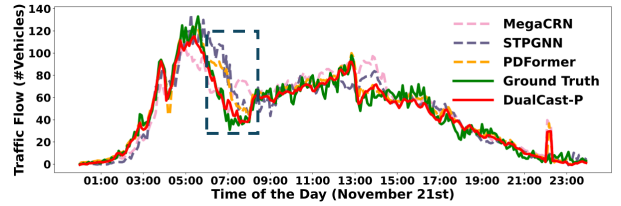
extraction. Here, we apply only the dual-branch structure and its corresponding loss functions to STTN, without incorporating the cross-attention mechanism. We denote this variant as **STTN-dual**. As Table VII shows, STTN-dual consistently outperforms STTN on all datasets. Importantly, STTN-dual also achieves larger improvements at complex times, which again confirms that our proposed dual-branch structure can effectively handle complex situations (aperiodic events).

#### D. Parameter and Case study.

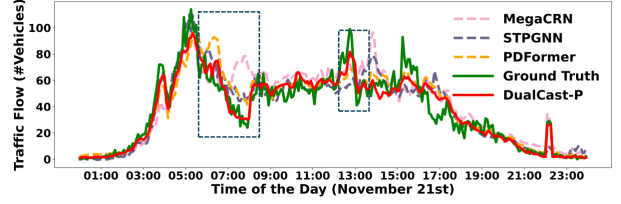
**Parameter study.** We study the impact of the hyper-parameters in our final loss function (Eq. 16), namely  $\alpha$ ,  $\beta$ , and  $\gamma$ . Figs. 12 to 14 show that, overall, the forecasting errors stay at low values consistently when the hyper-parameters in the loss vary. Such results confirm that the three losses jointly contribute to the model accuracy and that DualCast is robust without the need for heavy hyper-parameter tuning.

**Case study.** We conduct two case studies below.

*Responding to traffic accidents.* We cross-reference the car crash reports in Melbourne [49] with the Melbourne dataset and found one car crash during the time frame of the dataset. In Fig. 8(b), we visualise the ground-truth traffic flow observations and the forecasting results (15-minutes ahead of time) of DualCast-G (the best models for this dataset) and its



(a) Sensor #72 on PEMS03



(b) Sensor #97 on PEMS03

Fig. 15: A case study of responding to sudden changes (highlighted in rectangles) in traffic on PEMS03 on Nov. 21.

vanilla counterpart GMAN, and top-2 best baseline models, i.e., STPGNN and MegaCRN, at the sensor nearest to the accident. As the figure shows, DualCast-G responds quickly to the change in traffic flow caused by the car accident at around 8:00, generating forecasting results closer to the ground truth than both baseline models.

*Responding to sudden changes in traffic.* On the PEMS datasets, we do not have ground-truth traffic events. Instead, we inspected the ground-truth traffic observations and found two representative sensors (Sensors #72 and #97) of PEMS03 with sudden changes in traffic patterns on November 21st, 2018. Fig. 15 plots the ground-truth traffic flow values and the forecasts made an hour ahead by MegaCRN, STPGNN, PDFormer, and DualCast-P (since PDFormer is the stronger model on PEMS data) at Sensors #72 and #97. We see that DualCast-P generates forecasts that are the closest to the ground truth, with larger performance gaps at times with sudden changes in the traffic condition, again highlighting the strength of DualCast.

## VI. CONCLUSION AND FUTURE WORK

We proposed a framework named DualCast that enhances the robustness of self-attention-based traffic forecasting models, including the SOTA, in handling scenarios with complex environment contexts. DualCast takes a dual-branch structure to disentangle the impact of complex environment contexts, as guided by three loss functions. We further proposed a cross-time attention module to capture high-order spatial-temporal relationships. We performed experiments on real-world freeway and urban traffic datasets, where models powered by DualCast outperform their original versions by up to 9.6%. The best DualCast-based model outperforms the SOTA model by up to 2.6%, in terms of forecasting errors. For future work, we aim to integrate DualCast with non-attention-based models, such as CNN-based ones [50], in an effort to further enhance its general applicability.

## REFERENCES

- [1] X. Zhu, L. Zheng, C. J. Zhang, P. Cheng, R. Meng, L. Chen, X. Lin, and J. Yin, "Privacy-Preserving Traffic Flow Release with Consistency Constraints," in *ICDE*, 2024, pp. 1699–1711.
- [2] Z. Xu, L. Li, M. Zhang, Y. Xu, and X. Zhou, "Managing the Future: Route Planning Influence Evaluation in Transportation Systems," in *ICDE*, 2024, pp. 4558–4572.
- [3] M. Ma, J. Hu, C. S. Jensen, F. Teng, P. Han, Z. Xu, and T. Li, "Learning Time-aware Graph Structures for Spatially Correlated Time Series Forecasting," in *ICDE*, 2024, pp. 4435–4448.
- [4] J. Qin, Y. Jia, Y. Tong, H. Chai, Y. Ding, X. Wang, B. Fang, and Q. Liao, "MUSE-Net: Disentangling Multi-Periodicity for Traffic Flow Forecasting," in *ICDE*, 2024, pp. 1282–1295.
- [5] M. Li and Z. Zhu, "Spatial-Temporal Fusion Graph Neural Networks for Traffic Flow Forecasting," in *AAAI*, 2021, pp. 4189–4196.
- [6] S. Guo, Y. Lin, N. Feng, C. Song, and H. Wan, "Attention Based Spatial-Temporal Graph Convolutional Networks for Traffic Flow Forecasting," in *AAAI*, 2019, pp. 922–929.
- [7] Z. Fang, Q. Long, G. Song, and K. Xie, "Spatial-Temporal Graph ODE Networks for Traffic Flow Forecasting," in *KDD*, 2021, pp. 364–373.
- [8] C. Song, Y. Lin, S. Guo, and H. Wan, "Spatial-Temporal Synchronous Graph Convolutional Networks: A New Framework for Spatial-Temporal Network Data Forecasting," in *AAAI*, 2020, pp. 914–921.
- [9] Z. Wu, S. Pan, G. Long, J. Jiang, and C. Zhang, "Graph WaveNet for Deep Spatial-Temporal Graph Modeling," in *IJCAI*, 2019, pp. 1907–1913.
- [10] J. Qi, Z. Zhao, E. Tanin, T. Cui, N. Nassir, and M. Sarvi, "A Graph and Attentive Multi-Path Convolutional Network for Traffic Prediction," *IEEE Transactions on Knowledge and Data Engineering*, pp. 6548–6560, 2022.
- [11] M. Xu, W. Dai, C. Liu, X. Gao, W. Lin, G.-J. Qi, and H. Xiong, "Spatial-Temporal Transformer Networks for Traffic Flow Forecasting," *arXiv preprint arXiv:2001.02908*, 2020.
- [12] C. Zheng, X. Fan, C. Wang, and J. Qi, "GMAN: A Graph Multi-Attention Network for Traffic Prediction," in *AAAI*, 2020, pp. 1234–1241.
- [13] J. Jiang, C. Han, W. X. Zhao, and J. Wang, "PDFormer: Propagation Delay-Aware Dynamic Long-Range Transformer for Traffic Flow Prediction," in *AAAI*, 2023, p. 4365–4373.
- [14] Y. Tang, L. Qi, F. Xie, X. Li, C. Ma, and M.-H. Yang, "PredFormer: Transformers Are Effective Spatial-Temporal Predictive Learners," *arXiv preprint arXiv:2410.04733*, 2024.
- [15] H. Liu, Z. Dong, R. Jiang, J. Deng, J. Deng, Q. Chen, and X. Song, "Spatio-temporal Adaptive Embedding Makes Vanilla Transformer SOTA For Traffic Forecasting," in *CIKM*, 2023, pp. 4125–4129.
- [16] S. V. Kumar and L. Vanajakshi, "Short-Term Traffic Flow Prediction Using Seasonal ARIMA Model with Limited Input Data," *European Transport Research Review*, pp. 21:1–21:9, 2015.
- [17] G. E. P. Box, G. M. Jenkins, G. C. Reinsel, and G. M. Ljung, *Time Series Analysis: Forecasting and Control*. John Wiley & Sons, 2015.
- [18] Y. Tian and L. Pan, "Predicting Short-term Traffic Flow by Long Short-term Memory Recurrent Neural Network," in *IEEE International Conference on Smart City/SocialCom/SustainCom*, 2015, pp. 153–158.
- [19] Z. Zhao, W. Chen, X. Wu, P. C. Chen, and J. Liu, "LSTM Network: A Deep Learning Approach for Short-Term Traffic Forecast," *IET Intelligent Transport Systems*, pp. 68–75, 2017.
- [20] Y. Li, R. Yu, C. Shahabi, and Y. Liu, "Diffusion Convolutional Recurrent Neural Network: Data-Driven Traffic Forecasting," in *ICLR*, 2018.
- [21] X. Wang, Y. Ma, Y. Wang, W. Jin, X. Wang, J. Tang, C. Jia, and J. Yu, "Traffic Flow Prediction via Spatial Temporal Graph Neural Network," in *WWW*, 2020, pp. 1082–1092.
- [22] Z. Wu, S. Pan, G. Long, J. Jiang, X. Chang, and C. Zhang, "Connecting the Dots: Multivariate Time Series Forecasting with Graph Neural Networks," in *KDD*, 2020, pp. 753–763.
- [23] W. Kong, Z. Guo, and Y. Liu, "Spatio-Temporal Pivotal Graph Neural Networks for Traffic Flow Forecasting," in *AAAI*, 2024, pp. 8627–8635.
- [24] B. Yu, H. Yin, and Z. Zhu, "Spatio-Temporal Graph Convolutional Networks: A Deep Learning Framework for Traffic Forecasting," in *IJCAI*, 2018, pp. 3634–3640.
- [25] Y. Jin, K. Chen, and Q. Yang, "Selective Cross-City Transfer Learning for Traffic Prediction via Source City Region Re-Weighting," in *KDD*, 2022, pp. 731–741.
- [26] R. Jiang, Z. Wang, J. Yong, P. Jeph, Q. Chen, Y. Kobayashi, X. Song, S. Fukushima, and T. Suzumura, "Spatio-Temporal Meta-Graph Learning for Traffic Forecasting," in *AAAI*, 2023, pp. 8078–8086.
- [27] X. Su, J. Qi, E. Tanin, Y. Chang, and M. Sarvi, "Spatial-Temporal Forecasting for Regions without Observations," in *EDBT*, 2024, pp. 488–500.
- [28] C. Zheng, X. Fan, C. Wang, J. Qi, C. Chen, and L. Chen, "INCREASE: Inductive Graph Representation Learning for Spatio-Temporal Kriging," in *WWW*, 2023, pp. 673–683.
- [29] S. Li, Y. Cui, L. Li, W. Yang, F. Zhang, and X. Zhou, "ST-ABC: Spatio-Temporal Attention-Based Convolutional Network for Multi-Scale Lane-Level Traffic Prediction," in *ICDE*, 2024, pp. 1185–1198.
- [30] Y. Xia, Y. Liang, H. Wen, X. Liu, K. Wang, Z. Zhou, and R. Zimmermann, "Deciphering Spatio-Temporal Graph Forecasting: A Causal Lens and Treatment," *NeurIPS*, pp. 37 068–37 088, 2023.
- [31] Y. Zhao, X. Luo, W. Ju, C. Chen, X.-S. Hua, and M. Zhang, "Dynamic Hypergraph Structure Learning for Traffic Flow Forecasting," in *ICDE*, 2023, pp. 2303–2316.
- [32] Z. Wang, R. Jiang, H. Xue, F. D. Salim, X. Song, and R. Shibasaki, "Event-aware Multimodal Mobility Nowcasting," in *AAAI*, 2022, pp. 4228–4236.
- [33] X. Chen, H. Chen, Y. Yang, H. Wu, W. Zhang, J. Zhao, and Y. Xiong, "Traffic Flow Prediction by an Ensemble Framework with Data Denoising and Deep Learning Model," *Physica A: Statistical Mechanics and Its Applications*, p. 125574, 2021.
- [34] C. Chang, C.-T. Chan, W.-Y. Wang, W.-C. Peng, and T.-F. Chen, "TimeDRL: Disentangled Representation Learning for Multivariate Time-Series," in *ICDE*, 2024, pp. 625–638.
- [35] K. Sun, P. Liu, P. Li, and Z. Liao, "ModWaveMLP: MLP-Based Mode Decomposition and Wavelet Denoising Model to Defeat Complex Structures in Traffic Forecasting," in *AAAI*, 2024, pp. 9035–9043.
- [36] Y. Fang, Y. Qin, H. Luo, F. Zhao, B. Xu, L. Zeng, and C. Wang, "When Spatio-Temporal Meet Wavelets: Disentangled Traffic Forecasting via Efficient Spectral Graph Attention Networks," in *ICDE*, 2023, pp. 517–529.
- [37] J. Deng, X. Chen, R. Jiang, X. Song, and I. W. Tsang, "ST-Norm: Spatial and Temporal Normalization for Multi-variate Time Series Forecasting," in *KDD*, 2021, pp. 269–278.
- [38] K. Yi, Q. Zhang, W. Fan, H. He, L. Hu, P. Wang, N. An, L. Cao, and Z. Niu, "FourierGNN: Rethinking Multivariate Time Series Forecasting from a Pure Graph Perspective," in *NeurIPS*, 2024, pp. 69 638–69 660.
- [39] Z. Zhou, Q. Huang, K. Yang, K. Wang, X. Wang, Y. Zhang, Y. Liang, and Y. Wang, "Maintaining the Status Quo: Capturing Invariant Relations for OOD Spatiotemporal Learning," in *KDD*, 2023, pp. 3603–3614.
- [40] J. Arevalo, T. Solorio, M. Montes-y Gómez, and F. A. González, "Gated Multimodal Units for Information Fusion," *arXiv preprint arXiv:1702.01992*, 2017.
- [41] D. L. Davies and D. W. Bouldin, "A Cluster Separation Measure," *IEEE Transactions on Pattern Analysis and Machine Intelligence*, pp. 224–227, 1979.
- [42] S. Huang, Y. Song, J. Zhou, and Z. Lin, "Tailoring Self-Attention for Graph via Rooted Subtrees," in *NeurIPS*, 2023, pp. 73 559–73 581.
- [43] California Transportation Agencies (CalTrans) Performance Measurement System (PeMS). (2001) <https://pems.dot.ca.gov>.
- [44] J. Wang, J. Jiang, W. Jiang, C. Li, and W. X. Zhao, "LibCity: An Open Library for Traffic Prediction," in *SIGSPATIAL*, 2021, pp. 145–148.
- [45] Y. Jin, K. Chen, and Q. Yang, "Transferable Graph Structure Learning for Graph-based Traffic Forecasting across Cities," in *KDD*, 2023, pp. 1032–1043.
- [46] X. Liu, Y. Liang, C. Huang, Y. Zheng, B. Hooi, and R. Zimmermann, "When do Contrastive Learning Signals Help Spatio-temporal Graph Forecasting?" in *SIGSPATIAL*, 2022, pp. 5:1–5:12.
- [47] M. Karacasu, A. Er, S. Bilgic, and H. B. Barut, "Variations in Traffic Accidents on Seasonal, Monthly, Daily and Hourly Basis: Eskisehir Case," *Procedia-Social and Behavioral Sciences*, pp. 767–775, 2011.
- [48] M. Ruikar, "National Statistics of Road Traffic Accidents in India," *Journal of Orthopaedics, Traumatology and Rehabilitation*, pp. 1–6, 2013.
- [49] Victoria Road Crash Data. (2023) <https://discover.data.vic.gov.au/dataset/victoria-road-crash-data>.
- [50] T. Bogaerts, A. D. Masegosa, J. S. Angarita-Zapata, E. Onieva, and P. Hellinckx, "A Graph CNN-LSTM Neural Network for Short and Long-Term Traffic Forecasting Based on Trajectory Data," *Transportation Research Part C: Emerging Technologies*, pp. 62–77, 2020.